

# Direct Observation of Topological Protected Edge States in Slow-Light

Yu-Han Chang,<sup>1</sup> Raul A. Robles Robles,<sup>2</sup> Vanna Christmas Silalahi,<sup>1</sup> Cen-Shawn Wu,<sup>3</sup> Gang Wang,<sup>4</sup> Giulia Marcucci,<sup>5,6</sup> Laura Pilozzi,<sup>6</sup> Claudio Conti,<sup>5,6</sup> Ray-Kuang Lee,<sup>2,7</sup> and Watson Kuo<sup>1,7,\*</sup>

<sup>1</sup>*Department of Physics, National Chung Hsing University, Taichung 402, Taiwan*

<sup>2</sup>*Institute of Photonics Technologies, National Tsing Hua University, Hsinchu 300, Taiwan*

<sup>3</sup>*Department of Physics, National Chang-Hua University of Education, Changhua 500, Taiwan*

<sup>4</sup>*School of Physical Science and Technology, Soochow University, Suzhou 215006, China*

<sup>5</sup>*Department of Physics, University Sapienza, Rome 00185, Italy*

<sup>6</sup>*Institute for Complex Systems, National Research Council (ISC-CNR), Rome 00185, Italy*

<sup>7</sup>*Center for Quantum Technology, Hsinchu 30013, Taiwan*

We use split-ring resonators to demonstrate topologically protected edge states in the Su-Schrieffer-Heeger model experimentally, but in a slow-light wave with the group velocity down to  $\sim 0.1$  of light speed in free space. A meta-material formed by an array of complementary split-ring resonators with controllable hopping strength enables the direct observation in transmission and reflection of non-trivial topology eigenstates, including a negative phase velocity regime. By rotating the texture orientation of the diatomic resonators, we can explore all the band structures and unveil the onset of the trivial and non-trivial protected eigenmodes at GHz frequencies, even in the presence of non-negligible loss. Our system realizes a fully tunable and controllable artificial optical system to study the interplay between topology and slow-light towards applications in quantum technologies.

Composited by dimers with staggered hopping amplitudes, a topological phase transition can be revealed in the Su-Schrieffer-Heeger (SSH) model owing to the existence of Zak phase associated with zero Berry curvature [1, 2]. Using the SSH model, people have illustrated the difference between bulk and boundary, chiral symmetry, adiabatic equivalence, topological invariants, and bulk-boundary correspondence [3]. Through the analogy in single-particle Hamiltonian, topologically non-trivial zero or  $\pi$  modes can also be observed in photonic systems, through a periodically setting on the confined potentials [4–7]. With the topologically protected edge states, we can implement new types of lasing mode [8] and optical control [9] even under continuous deformations.

Unlike the conventional optical structures formed by waveguide and resonators, one can design *meta-materials* to manipulate waves of electromagnetic radiation in a manner not observed in bulk materials. By properly engineering the unit cell, also known as artificial atoms, for example, media can possess simultaneous negative permittivity and negative permeability, resulting in a left-handed refractive index [10, 11]. In particular, the split-ring resonator (SRR) [12, 13] has provided an experimental platform to demonstrate magnetoinductive, electroinductive, retarded waves, and slow-light [14–18].

Even though the topologically protected edge state in one-dimension (1D) system is a discretized state inside the gap, a question arises on its group velocity when excited in slow-light meta-materials. In this Letter, we address this question by implementing the SSH model in an array of dimers with SSR and its counterpart, the complementary split-ring resonator (CSRR) [19]. In addition to the known approach by varying the separation between

two adjacent waveguides or resonators, the orientation of SRRs provides a feasible degree of freedom to manipulate the inter-resonator coupling strength [20–23]. Now, with the negative permittivity and negative permeability, supported respectively by SRRs and CSRRs, one can realize a left-handed meta-materials for microwave propagating with a negative phase velocity. With a proper setting on the intra-cell and inter-cell coupling strengths between SRRs and CSRRs, a photonic band gap in the passband is measured when the inversion symmetry is broken, as well as a very slow group velocity is supported, down to  $\sim 0.01$  of light speed in free space. Then, an even number of resonators are fabricated to illustrate experimentally non-trivial and trivial topologically protected edge states. By directly measuring the reflection and transmission spectra, we observe the Zak phase to support the existence of topological edge states in meta-materials. Non-trivial topologically protected edge states are directly observed with a group velocity  $\sim 13.6 \times 10^6$  m/s. As the slow-light has played an important role for studying photon-atom interaction, as well as for quantum memories, our system provides a fully tunable and controllable platform to study the interplay between topology and meta-material.

As schematic in Fig. 1(a), we study a 1D array composed by a finite number of dimer lattices in the diatomic basis, denoted as  $A$  and  $B$ . The implementation of SSH model is realized by combining SRRs and CSRRs together, but fabricated in the upper and lower layers, respectively, as illustrated in Fig. 1(b). By bonding these two interleaved layers close enough, with a controllable separation, an effective 1D array can be implemented to realize the Su-Schrieffer-Heeger model. With the images taken from the top and bottom, as shown in Figs. 1(c) and (d), one can clearly see the split-ring structures within the empty background in the upper layer; while the complementary structures in the lower layers.

\*Electronic address: wkuo@phys.nchu.edu.tw

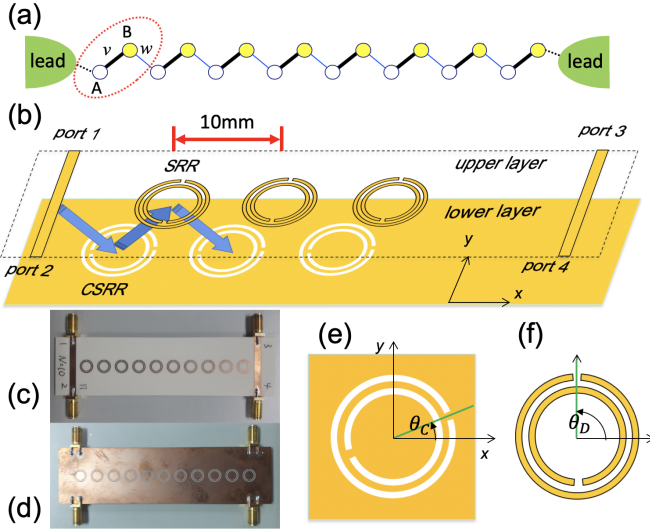


FIG. 1: (a) A schematic of the SSH model for 1D microwave propagation in dimer lattices, denoted as  $A$  and  $B$ . The red box marks the unit cell of “diatomic basis”. (b) The implementation of the SSH model is realized by combining split-ring resonators (SRRs) and complementary split-ring resonators (CSRRs), illustrated in (e) and (f), in an array structure. The SRRs are fabricated in the upper layer, as shown in the real image taken from the top (c); while the CSRRs are fabricated in the lower layer, as shown in the image taken from the bottom (d). By varying the orientation of SRRs and CSRRs, as illustrated in (e) and (f), we can manipulate the coupling strengths for the intra- and inter-cells, denoted as  $v$  and  $w$ , respectively. The two leads in the front and end nodes shown in (a) are implemented by two transmission lines in (b), denoted with the input port 1, reflection port 2, and transmissions ports 3 and 4.

In addition to the dimer unit, we manipulate the coupling strengths, denoted as  $v$  and  $w$ , for the intra- and inter-cells by varying the orientation of SRRs and CSRRs, as denoted as  $\theta_S$  and  $\theta_C$  in Figs. (e) and (f), respectively. Moreover, to link the 1D lattice model to the measurement on the transmission and reflection spectra, as illustrated in Fig. 1(a), we also introduce two leads in the front and end nodes. With the help of two transmission lines, as shown in Fig. 1(b), here, we define the input (port 1), reflection (port 2), and transmissions ports (3 and 4).

To illustrate the topologically protected edge states supported in the SSH model, one can consider each ring as a single harmonic oscillator coupled to the adjacent oscillators. As a generalized SSH model by including the lossy effect, the equations of motion for the electric field amplitude  $x$  at the  $j$ -th site can be described as

$$\ddot{x}_j = -\omega_j^2 x_j - \gamma_j \dot{x}_j + \kappa_{j-1} x_{j-1} + \kappa_{j+1} x_{j+1}, \quad (1)$$

where the site index  $j$  runs from 1 to  $N$  for the total number of SRRs and CRRs. Here, we also introduce  $\omega_j$  as the natural frequency of the oscillator,  $\gamma_j$  as the damping coefficient (for the ring resonator is linked to resis-

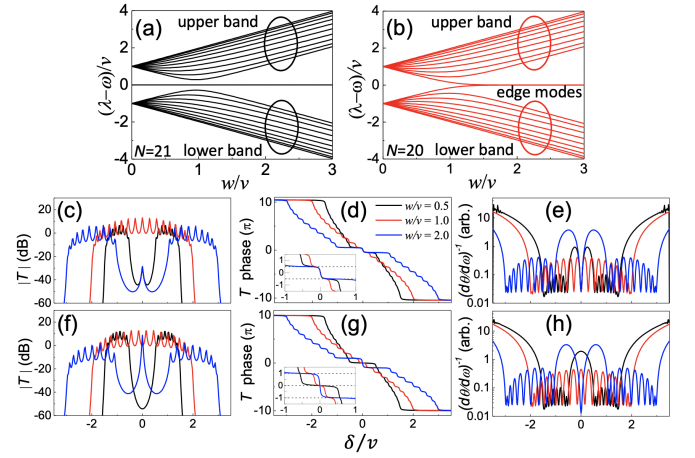


FIG. 2: The eigen-energies of our 1D SSH model are shown as a function of the ratio between the inter- and intra-cell hopping constants,  $w/v$ , for (a) odd number ( $N = 21$ ), and (b) even number ( $N = 20$ ) of the total lattices. The corresponding (c, f) transmission spectra  $|T|$  (in dB scale), (d, g) phase change, and (e, h) group velocity  $(d\theta/d\omega)^{-1}$  are depicted for odd and even numbers, shown in (c-e) and (f-h), as a function of the normalized detuning frequency  $\delta/v$ , for  $w/v = 0.5, 1.0$ , and  $2.0$  depicted in Black-, Red, and Blue-curves, respectively. The insets in (d) and (g) show the phase change near the zero-detuning region, i.e.,  $\delta/v = \pm 1$ .

tance loss), and  $\kappa_{j\pm 1}$  as the coupling constants between two adjacent oscillators. The solutions for a particular frequency  $\omega$  can be expressed by noting  $x_j = A_j e^{-i\omega t}$ . Here, the dimer unit  $A$  and  $B$  are characterized by their resonance frequencies  $\omega_A$  and  $\omega_B$ , which are the same  $\omega_A = \omega_B$  for the SSH model, but can be different for the Rice-Mele model [24]. Additionally, the staggered coupling coefficients are assumed to be different for intra-cell and inter-cell, denoted as  $\kappa_A$  and  $\kappa_B$ .

By defining  $v \equiv \kappa_A/2\omega_A$ ,  $w \equiv \kappa_B/2\omega_A$ , along with  $\gamma_i \ll \omega \sim \omega_i$ , as the band structure of the system shown in Figs. 2(a) and (b), the eigen-energies, in terms of  $(\lambda - \omega)/v \equiv \delta/v$ , are depicted as a function of the ratio between the inter- and intra-cell hopping constants,  $w/v$  or equivalently  $\kappa_B/\kappa_A$ , for (a) odd number ( $N = 21$ ), and (b) even number ( $N = 20$ ) of the total lattices. In addition to the two branches of band, i.e., upper and lower bands, for an odd value of  $N$ , a defect-mode with the zero eigen-energy always exists no matter what is the value of  $w/v$ , as shown in Fig. 2(a). Nevertheless, for an even number of  $N$ , non-trivial topological edge states, i.e., the zero-modes, only emerge when  $w/v > 1$ , as shown in Fig. 2(b).

In response to directly probe these non-trivial topologically protected edge states experimentally through the transmission spectroscopy, one can add a driving force on the model system in Eq. (1) at the first site  $x_1$  and measure the response at the last site  $x_N$ . The corresponding transmission amplitudes  $|T|$  (in dB scale), are depicted in Figs. 2(c) and (f) for an odd ( $N = 21$ ) and

an even ( $N = 20$ ) number of  $N$ , respectively, as a function of the normalized detuning frequency  $\delta/v$ . Here, three values of the ratio  $w/v$  are chosen. When  $N = 21$ , one can see from Fig. 2(c) that the resulting transmission features a single passband for  $w/v = 1$  as shown in the Red-curve; while this passband is split into two with a gap region in between for  $w/v \neq 1$ , as shown in Black- and Blue-curves for  $w/v = 0.5$  and  $2$ , respectively. Moreover, to take the dissipation into consideration, lossy effects are also included in the calculations, by setting  $\gamma_A = \gamma_B = \gamma = 0.02v$ . As one can see that the transmission spectra are robust even with the introduction of non-negligible losses. Some ripples in the transmission spectrum can be easily identified as only a finite number of resonators is considered. With the comparison between Figs. 2(c) and (f), topologically non-trivial states, i.e., zero-modes, only emerge at the center of band gap when the number of total lattice is even and  $w/v > 1$ .

In addition to the transmission amplitudes, the corresponding phase changes are also shown in Figs. 2(d) and (g) for the odd and even number of  $N$ , respectively. Near the zero-detuning region, i.e.,  $\delta/v = \pm 1$ , a phase jump of  $\pi$ , from  $-\pi/2$  to  $\pi/2$ , can be seen from the inset of Fig. 2(d), accounting for the trivial topological phase. However, as shown in the Blue-curve of Fig. 2(g), when  $w/v = 2.0 > 1$ , a phase jump of  $2\pi$ , from two Zak phases in  $\pm\pi$ , appears for the existence of the non-trivial topologically protected edge state. Instead, when  $w/v = 0.5 < 1$ , the phase change remains a constant in the gap region, as shown in the Black-curve. Furthermore, it is known that the group velocity is proportional to the slope of the dispersion curve, i.e.,  $v_g = d\omega/dk = L(d\theta/d\omega)^{-1}$ , with  $L$  denoting the length of our 1D array. By taking the derivative of the phase curves in Figs. 2(d) and (g), for the odd and even number of lattices, respectively, we depict the inverse of the derivative of phase change, i.e.,  $(d\theta/d\omega)^{-1}$ , relating to the group velocity in Figs. 2(e) and (f). One can see that, even though the lowest group velocities happen near the two band edges, both the supported trivial and non-trivial topologically protected edge states have a slower group velocity inside the gap region. In short, the non-trivial topologically protected edge states indeed propagate in slow-light.

Now, let us come to the experimental implementation of our 1D SSH array on the substrate Roger 4003C, which has the thickness 1.6 mm and with copper used as the metallic part in 0.035 mm thickness on it. The resonators are designed with 7.6 mm in diameter, 0.4 mm in line width, along with 0.4 mm between two rings, 0.4 mm for the ring gaps, and 10 mm for the lattice constant. For the  $N = 20$  sample, we have  $L = 106.2$  mm in total length from the left lead to the right one. It is known that one can manipulate the coupling strengths between SRRs by angle of rotations [25]. Moreover, for the coupled SRR and CSRR, the texture of orientation produces a great impact on the inter-resonator coupling strength [26]. As illustrated in Figs. 1(e) and (f), for a fixed angle of rota-

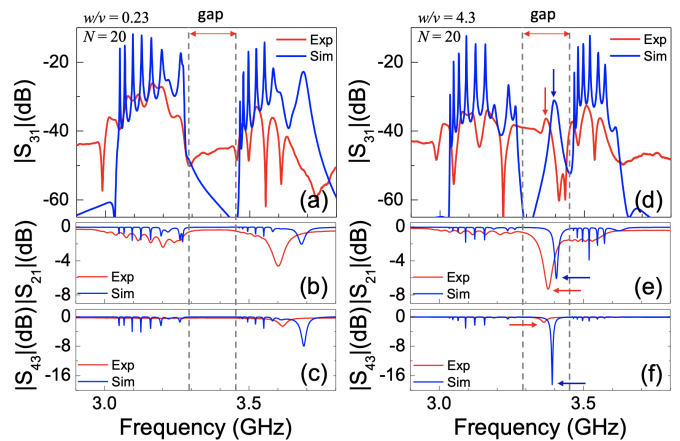


FIG. 3: (a, d) Measured transmission  $|S_{31}|$  and reflection spectra: with the injection (b, e) from the left lead  $|S_{21}|$  and (c, f) from the right lead  $|S_{43}|$  in (c, f), are depicted in Red-curves for an even number of the total rings,  $N = 20$ . Numerical results obtained from finite-element simulations are also depicted in Blue-curves. Here, the orientations of SRRs and CSRRs are rotated at the angles: (a-c)  $(210^\circ, 290^\circ)$  and (d-f)  $(30^\circ, 110^\circ)$ , with the estimated values of  $w/v = 0.23$  and  $4.3$ , respectively. Within the frequency gap between two split passbands, from 3.25 to 3.40 GHz, the topologically protected edge states produce an additional resonance peak in the (d) transmission spectrum, or a dip in the (e, f) reflection spectra, as indicated by the arrow sign.

tion in CSRR,  $\theta_C$ , the inter-resonator coupling strength can be varied from 30 MHz to 400 MHz with respect to the angle of rotation in SRR,  $\theta_S$ . To extract the magnitude of coupling strengths in our diatomic cell, simulation results obtained by finite-element simulations are also applied to fit the experimental data, in order to estimate the values of ratio between inter- and intra-cell coupling strengths.

With the help of experimental parameters extracted from our previous work [26], in the following we demonstrate the direct observation of non-trivial topologically protected edge states for microwave propagation in our 1D array. Here, an even number of the total lattice is fabricated, i.e.,  $N = 20$ , for two sets of the orientations of SRRs and CSRRs rotated at the angles  $(\theta_S, \theta_C)$ : (a-c)  $(210^\circ, 290^\circ)$  and (d-f)  $(30^\circ, 110^\circ)$ . As the selected angles in these two cases are supplementary, the coupling strengths  $v$  and  $w$  are simply interchanged, with the estimated values of  $w/v = 0.23$  and  $4.3$ , respectively. For the topologically trivial case, a clear frequency gap between two split passbands is observed in both the transmission and reflection spectra from 3.25 to 3.40 GHz, as shown in Figs. 3(a-c). Instead, as shown in Fig. 3(d) for the transmission spectrum obtained by directly measuring  $S_{31}$ , the topologically protected edge states produce the additional resonance peak in the gap region, as indicated by the arrow sign. Moreover, to manifest such a topologically non-trivial state, in Figs. 3(e) and (f), we also perform the measurements on the reflection spectrum from

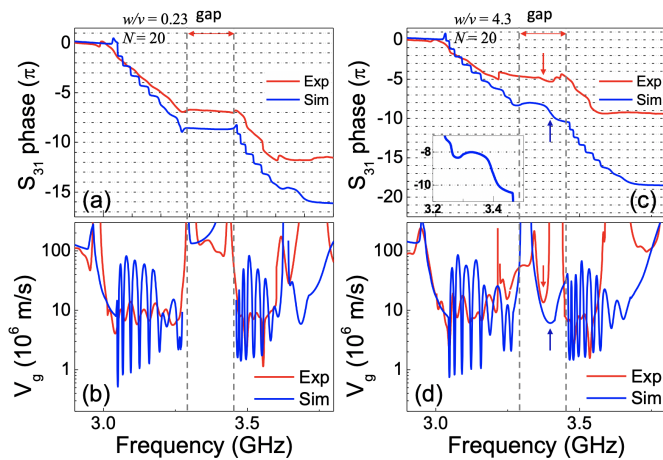


FIG. 4: (a, c) Measured phase spectra from the scattering coefficient  $S_{31}$  and (b, d) the corresponding group velocity  $V_g$  are depicted in Red-curves for an even number of the total rings,  $N = 20$ . Numerical results obtained from finite-element simulations are also depicted in Blue-curves. The inset of (c) is the enlarged gap region, which illustrates a phase difference of  $2\pi$ .

the scattering coefficients  $|S_{21}|$  and  $|S_{43}|$ , respectively, for the injection from the left and right leads, respectively. Even though fabrication errors introduce inevitable discrepancy in the measured spectrum, a clear resonant dip can be seen in the both reflection spectra, indicating the robustness of topologically protected edge states. In Fig. 3, we also depict numerical results obtained from finite-element simulations in Blue-curves, which not only give good agreement to all the experimental data, but also reveal the fine structure from the oscillation peaks related to the number of resonators.

In order to demonstrate that our 1D arrays formed by SRRs and CSRRs can work as meta-materials, we also perform the measurement on the phase of the scattering parameter  $S_{31}$ , as shown in Red-curves in Fig. 4. To further unveil the onset of the trivial and non-trivial protected edge states, simulation results from finite-element method are also depicted in Blue-curves as a comparison. In addition to the negative slope for the phase measurement with respect to the frequency, in the gap region, a plateau with the constant phase change can be easily seen for the trivial case when  $w/v = 0.23$ , as shown in Fig. 4(a). Once again, our numerical simulations depicted in Blue-curves not only give good agreement to the measured phase change, but also reveal a stair-shape for the phase change inside the two passbands. Each discrete phase drop counts a  $\pi$  phase change, representing a resonance peak from the individual resonator. However, when  $w/v = 4.3$ , the existence of the non-trivial

topological states emerge in the gap region, which modify the original plateau, as shown in Fig. 4(c). As the inset shows, a  $2\pi$  phase change from the phase difference between two Zak phase  $\pm\pi$ , can be clearly seen for the supported topologically protected edge state in the gap region. The observed state indeed is a non-trivial zero mode.

Moreover, from the measured and simulated phase data, in Figs. 4(b) and (d), we also show the corresponding group velocity measurement, for the trivial and non-trivial topologically protected edge states, respectively. Compared to the theoretical results given in Fig. 2(h), when  $w/v = 0.23 < 1$  as shown in Fig. 4(b), the wave in the two split passbands propagates in a slow group velocity down to  $1.14 \times 10^6$  m/s,  $\sim 0.01$  of light speed in the free space. On the contrary, when  $w/v = 4.3 > 1$  as shown in Fig. 4(d), for the non-trivial topologically protected edge states supported inside the gap region, a significant dip in the measured group velocity, as well as in the simulated one, can be clearly identified, indicating a much lower group velocity than the light speed. Our results give a direct observation of the topologically protected edge states in slow-light, with the measured group velocity  $\sim 13.6 \times 10^6$  m/s.

To sum up, we propose and study 1D left-handed meta-materials based on interleaved split-ring resonators and complementary split ring resonators. The microwave propagation has a negative phase velocity and a very slow group velocity, down to  $\sim 0.01$  of light speed in free space. By varying the orientation texture, we realize the Su-Schrieffer-Heeger model for the electromagnetic waves in meta-material. The non-trivial topologically protected edge states are directly observed in the transmission and reflection spectra, with the group velocity  $\sim 13.6 \times 10^6$  m/s. Our results pave the way to study photon-atom interaction with topological photonics, which could overcome the difficulty in using photonic crystals due to the mismatch of the lattice constant and the feature size of an artificial atom. In addition, the success of the tight-binding model infers that such a diatomic basis may produce very rich exotic topological states when built into the Rice-Mele model or a two-dimensional system.

We are grateful to the National Center for High-performance Computing for computer time and facilities. Fruitful discussions with C. C. Huang and W. H. Chang are acknowledged. G.W. acknowledges the financial supports from National Natural Science Foundation of China (11604231); Natural Science Foundation of Jiangsu Province (BK20160303). This work is financially supported by the Ministry of Science and Technology, Taiwan under grant No.106-2112-M-005-007, 105-2628-M-007-003-MY4, and Research Center for Sustainable Energy and Nanotechnology, NCHU.

[1] W. P. Su, J. R. Schrieffer, and A. J. Heeger, Phys. Rev. B **22**, 2099 (1980).

[2] A. J. Heeger, S. Kivelson, J. R. Schrieffer, and W. P. Su,

- Rev. Mod. Phys. **60**, 781 (1988).
- [3] J. K. Asboth, L. Oroszlany, and A. Palyi, “The Su-Schrieffer-Heeger (SSH) Model,” in *A Short Course on Topological Insulators*, Lecture Notes in Physics, vol. 919 (Springer, 2016).
- [4] A. B. Khanikaev, S. H. Mousavi, W.-K. Tse, M. Kargarian, A. H. MacDonald, and G. Shvets, “Photonic topological insulators,” *Nature Mat.* **12**, 233 (2013).
- [5] L. Lu, J. D. Joannopoulos, and M. Soljacic, “Topological photonics,” *Nature Photon.* **8**, 821 (2014).
- [6] M. C. Rechtsman, J. M. Zeuner, Y. Plotnik, Y. Lumer, D. Podolsky, F. Dreisow, S. Nolte, M. Segev, and A. Szameit, “Two-dimensional topological photonics,” *Nature* **496**, 196 (2013).
- [7] Q. Cheng, Y. Pan, H. Wang, C. Zhang, D. Yu, A. Gover, H. Zhang, T. Li, L. Zhou, and S. Zhu, “Observation of Anomalous  $\pi$  Modes in Photonic Floquet Engineering,” *Phys. Rev. Lett.* **122**, 173901 (2019).
- [8] M. Parto, S. Wittek, H. Hodaei, G. Harari, M. A. Bandres, J. Ren, M. C. Rechtsman, M. Segev, D. N. Christodoulides, and M. Khajavikhan, “Edge-Mode Lasing in 1D Topological Active Arrays,” *Phys. Rev. Lett.* **120**, 113901 (2018).
- [9] G. Marcucci, D. Pierangeli, A. J. Agranat, R.-K. Lee, E. DelRe, and C. Conti, “Topological control of extreme waves,” *Nature Comm.* **10**, 5090 (2019).
- [10] D. R. Smith, J. B. Pendry, and M. C. K. Wiltshire, “Metamaterials and Negative Refractive Index,” *Science* **305**, 788 (2004).
- [11] V. M. Shalaev, “Optical negative-index metamaterials,” *Nat. Photon.* **1**, 41 (2007).
- [12] R. A. Shelby, D. R. Smith, and S. Schultz, “Experimental verification of a negative index of refraction,” *Science* **292**, 77 (2001).
- [13] S. Linden, C. Enkrich, M. Wegener, J. Zhou, T. Koschny, and C. M. Soukoulis, “Magnetic Response of Metamaterials at 100 Terahertz,” *Science* **306**, 1351 (2004).
- [14] H. Liu, D. A. Genov, D. M. Wu, Y. M. Liu, J. M. Steele, C. Sun, S. N. Zhu, and X. Zhang, “Magnetic Plasmon Propagation Along a Chain of Connected Subwavelength Resonators at Infrared Frequencies,” *Phys. Rev. Lett.* **97**, 243902 (2006).
- [15] M. Beruete, F. Falcone, M. J. Freire, R. Marqus, and J. D. Baena, “Electroinductive waves in chains of complementary metamaterial elements,” *Appl. Phys. Lett.* **88**, 083503 (2006).
- [16] M. Navarro-Ca, M. Aznabet, M. Beruete, F. Falcone, O. El Mrabet, M. Sorolla, and M. Essaaidi, “Stacked complementary metasurfaces for ultraslow microwave metamaterials,” *Appl. Phys. Lett.* **96**, 164103 (2010).
- [17] F. Miyamaru, H. Morita, Y. Nishiyama, T. Nishida, T. Nakanishi, M. Kitano, and M. W. Takeda, “Ultrafast optical control of group delay of narrow-band terahertz waves,” *Sci. Rep.* **4**, 4346 (2004).
- [18] C. Wu, A. Khanikaev, and G. Shvets, “Broadband slow light metamaterial based on a double-continuum Fano resonance,” *Phys. Rev. Lett.* **106**, 107403 (2011).
- [19] F. Falcone, T. Lopetegi, M. A. G. Laso, J. D. Baena, J. Bonache, M. Beruete, R. Marqus, F. Martn, and M. Sorolla, “Babinet Principle Applied to the Design of Metasurfaces and Metamaterials,” *Phys. Rev. Lett.* **93**, 197401 (2004).
- [20] I. Sersic, M. Frimmer, E. Verhagen, and A. F. Koenderink, “Electric and Magnetic Dipole Coupling in Near-Infrared Split-Ring Metamaterial Arrays,” *Phys. Rev. Lett.* **103**, 213902 (2009).
- [21] H. Guo, N. Liu, L. Fu, T. P. Meyrath, T. Zentgraf, H. Schweizer, and H. Giessen, “Resonance hybridization in double split-ring resonator metamaterials,” *Opt. Exp.* **15**, 12095 (2017).
- [22] T. Li, R. X. Ye, C. Li, H. Liu, S. M. Wang, J. X. Cao, S. N. Zhu, and X. Zhang, “Structural-configured magnetic plasmon bands in connected ring chains,” *Opt. Exp.* **17**, 11486 (2009).
- [23] S. S. Seetharaman, C. G. King, I. R. Hooper, and W. L. Barnes, “Electromagnetic interactions in a pair of coupled split-ring resonators,” *Phys. Rev. A* **96**, 085426 (2017).
- [24] M. J. Rice and E. J. Mele, “Elementary excitations of a linearly conjugated diatomic polymer,” *Phys. Rev. Lett.* **49**, 1455 (1982).
- [25] J. Jiang, Z. Guo, Y. Ding, Y. Sun, Y. Li, H. Jiang, and H. Chen, “Experimental demonstration of the robust edge states in a split-ring-resonator chain,” *Opt. Express* **26**, 12891 (2018).
- [26] Y.-J. Lin, Y.-H. Chang, W.-C. Chien, and W. Kuo, “Transmission line metamaterials based on strongly coupled split ring/complementary split ring resonators,” *Opt. Exp.* **25**, 30395 (2017).